Journal of Membrane Science 632 (2021) 119374

Contents lists available at ScienceDirect

Journal of Membrane Science

journal homepage: http://www.elsevier.com/locate/memsci

Hollow-fiber membranes of block copolymers by melt spinning and selective swelling

Dinglei Zhong, Jiemei Zhou, Yong Wang *

State Key Laboratory of Materials-Oriented Chemical Engineering, College of Chemical Engineering, Nanjing Tech University, Nanjing, 211816, Jiangsu, PR China

ARTICLE INFO

Keywords:
Hollow-fiber membranes
Block copolymers
Melt spinning
Selective swelling
Clean production

ABSTRACT

Selective swelling of block copolymers has emerged as an efficient strategy to prepare ultrafiltration membranes with well-defined porosities. However, the application of this strategy is only limited to the preparation of flat-sheet membranes so far. Herein, we extend this selective swelling strategy, for the first time, to the preparation of hollow-fiber membranes (HFMs). A mechanically strong copolymer available at large scale, polysulfone-*block*-poly(ethylene glycol) (PSF-*b*-PEG), is employed as the membrane-forming polymer. The PSF-*b*-PEG melt without any diluters or additives exhibits good fluidity, enabling stable and continuous melt spinning of primary hollow fibers with dense fiber walls. Subsequent selective swelling in the mixture of *n*-propyl alcohol and acetone produces interconnected nanoporosities throughout the fiber walls, thus forming HFMs with PEG chains enriched on the membrane surface. The wall thicknesses as well as pore sizes, and thus the separation performances of the HFMs are tunable by changing the spinning and swelling parameters. In contrast to the strong hydrophobicity of HFMs prepared by cold stretching of polyolfins, our HFMs possess water-wettable surfaces due to the presence of PEG chains, and can be directly used in aqueous milieu. Because of the PSF-based skeleton and homogenous distribution of nanopores, the HFMs exhibit excellent tensile strengths up to 12.5 MPa, much higher than that of HFMs prepared by the commonly used phase inversion processes. Furthermore, the BSA rejection and water permeance of the HFMs currently can be tuned in the range of 29.9–88.2% and 13.7–119.3 L $m^{-2}{\cdot}h^{-1}{\cdot}bar^{-1}$, respectively, by changing the spinning and/or swelling parameters. Their performances are expected to enhance by optimizing the hollow fiber geometries and pore structures. This strategy neither uses any solvents to fluidize the polymer nor produces wastewater, and therefore is a "cleaner" process. This work not only extends the usages of selective swelling, but also establishes a new process to manufacture HFMs.

1. Introduction

Block copolymers (BCPs) have attracted significant interest mainly because of their ability to form well-defined nanostructures [1]. Based on the volume fractions and the Flory-Huggins interaction parameter between constituent blocks, the thermodynamically immiscible blocks of BCPs form periodic nanostructures including spheres, cylinders, gyroids, lamellas, etc [2–4]. This specific nature allows the fabrication of a variety of highly ordered nanostructured materials from BCPs. The design of membranes from BCPs has received much attention over the past decade [5]. Microphase separation of BCPs leads to well-ordered microdomains of the minority block homogeneously dispersed in the continuous phase of the majority block. Emptying the microdomains of the minority block produces nanoporous polymers with high ordering and narrow pore size distribution, which is the basic principle to prepare BCP-based ultrafiltration membranes for precise separation.

The strategies established for the preparation of porous structures from BCP materials mainly include selective degradation of etchable blocks or pre-incorporated components [6], self-assembly in combination with nonsolvent-induced phase separation (SNIPS) [7] and selective swelling-induced pore generation [8]. Following these strategies, a number of membranes have been prepared from a variety of BCPs. For example, researchers reported the preparation of asymmetric membranes with a thin isoporous surface on the top of a sponge-like support from polystyrene-*block*-poly(4-vinylpyridine) (PS-*b*-P4VP) *via* the SNIPS process [9]. By selective swelling thin films of amphiphilic BCPs, we prepared a series of membranes with controllable pore geometries ranging from interconnected networked pores to highly ordered cylindrical and slit-shaped pores [10–13]. Thanking to the narrowed pore size distribution and in situ hydrophilic pore walls endowed by

* Corresponding author.
E-mail address: yongwang@njtech.edu.cn (Y. Wang).

https://doi.org/10.1016/j.memsci.2021.119374
Received 21 February 2021; Received in revised form 16 April 2021; Accepted 20 April 2021
Available online 24 April 2021

surface-enriched polar blocks, these membranes exhibited excellent performance in both selectivity and permeability. The studies of BCP membranes are mainly focused on the flat-sheet geometry. However, some researchers have paid attention to other configurations in recent years, such as hollow-fiber membranes (HFMs) [14–17]. Compared to flat-sheet membranes, HFMs exhibit much higher packing density as a result of their hollow cylindrical geometry, and consequently higher productivity in separations [18]. Therefore, it is highly desired to manufacture BCPs into membranes in the form of hollow fibers.

Polymer HFMs are most extensively prepared by phase inversion processes, mainly including nonsolvent induced phase separation (NIPS) [19–21], and thermally induced phase separation (TIPS) [22,23]. In these processes, membrane-forming polymers are fluidized by dissolving in organic solvents together with additives or diluters. Macrophase separation of polymer solutions is induced by nonsolvent exposure or temperature drops, and leads to a polymer-thin phase and a polymer-rich phase, which end up with the porosity and the solid skeleton of the eventually produced membranes, respectively. Particularly, following the NIPS process, HFMs of BCPs have also been prepared by dry-jet wet spinning of BCP solutions. Abetz et al. executed the dry-jet wet spinning technique to prepare PS-*b*-P4VP HFMs [24]. During spinning, PS-*b*-P4VP experienced the self-assembly process *via* solvent evaporation regulated by gas flow between the spinneret and the coagulation bath and then completed the phase inversion in the coagulation bath, producing HFMs with uniform pores in the inner surface of the hollow fibers. Unfortunately, NIPS is a solvent-extensive process that requires large volume of organic solvents, and it generates copious intractable wastewater, which may cause environmental and safety risks. Additionally, as a solvent-free process, cold stretching has been used to produce HFMs of a few crystalline polymers, for example, polyethylene (PE) [25], polypropylene (PP) [26], and polytetrafluoroethylene (PTFE) [27]. The amorphous phases which are mechanically weaker than the crystalline phases in the polymer are cavitated during stretching, thus forming pores typically with an elongated shape. However, HFMs prepared by this stretching process are usually highly hydrophobic, and are suffering from low permeance and severe fouling if directly used in aqueous milieu. Clearly, these commonly used strategies cannot be directly used to prepare block copolymer HFMs following the pore-making mechanism of selective swelling. Furthermore, there is a strong need for new strategies to prepare HFMs.

Typically, in the selective swelling process, dense BCP films are simply soaked in a solvent, i.e., the swelling agent, that is selective to the minority blocks. Once the films are taken out from the solvent and dried, the nanoporous structure is obtained throughout the films [28]. In addition, the minority blocks spontaneously migrate to the membrane surface and pore walls during swelling, resulting in inherent hydrophilicity [29]. Mechanically, selective swelling-induced pore generation is not dependent on the shapes and dimensions of BCP materials. Indeed, we have demonstrated that selective swelling is also able to produce nanoporosities in BCPs in the form of nanofibers [30] and monoliths [31] in addition to thin films. Therefore, we anticipate that selective swelling should, in principle, be able to prepare BCP membranes in the geometry of hollow fibers. Two essential points to realize the preparation of BCP HFMs by selective swelling are the affordable BCP materials and the reliable process to manufacture the BCPs into the form of hollow fibers prior to produce pores by selective swelling. Fortunately, we recently built the capability to synthesize a type of amphiphilic BCPs, polysulfone-*block*-poly(ethylene glycol) (PSF-*b*-PEG), in the scale of >100 kg/batch at a reasonable cost [32]. Importantly, this copolymer has an excellent mechanical property as it is consisted of tough strong PSF blocks and flexible PEG blocks. As for the production of polymer hollow fibers, melt spinning is the most commonly used process.

Therefore, in this work we explore to establish the manufacturing of HFMs of PSF-*b*-PEG by a two-step process: (1) melt spinning to produce primal hollow fibers, and (2) selective swelling to generate pores in the hollow fibers. Melt spinning the PSF-*b*-PEG pellets to produce primal hollow fibers effectively avoids the use of organic solvents (Fig. 1). Selective swelling is based on the different swelling behavior of two blocks in the selective solvent. It is a physical, nondestructive process, and the swelling agent can be repeatedly used. More importantly, the pore size can be flexibly regulated by delicately changing the swelling parameters including temperature, duration, and the compositions of swelling agents, which allows the manufacturing of BCP HFMs with adjustable separation properties. This study, for the first time, demonstrates the feasibility of the preparation of BCP HFMs by selective swelling coupled with melt spinning, and it also provide a solution to produce HFMs in a solvent-less way.

2. Experimental section

2.1. Materials

PSF-*b*-PEG block copolymers were synthesized by Nanjing Bangding. The dispersity ($Đ_M$) of the copolymer is ~2.00; the PEG block has a molecular weight of ~20 kDa, and the weight ratio of the PEG block in the copolymer is ~21%. Acetone (>99.5%) was purchased from Sinopharm Chemical Reagent Co., Ltd. *N*-propyl alcohol (>99.0%) was obtained from Aladdin Chemical Reagent Co., Ltd. Phosphate buffered solution (PBS) tablets and bovine serum albumin (BSA, 98%, M_w = 66 kDa) were purchased from MP Biomedicals, LLC. All reagents were used without further purification. Deionized water (conductivity = 8–20 μs cm^{-1}) was used in all tests.

2.2. Preparation of HFMs

The PSF-*b*-PEG hollow fibers were produced by using a miniature twin-screw extruder (Xinshuo, WLG10G) equipped with a heated hollow-fiber spinneret. The schematic diagram of hollow-fiber spinneret orifices is shown in the inset of Fig. 1. D and d_1 represent the outer diameter and inner diameter of the annular orifice in the spinneret, respectively. d_2 represents the diameter of the inner channel. The annular orifice with gap width determined by D and d_1, was used to confine the flow of polymer melts driven by the extruder, and there were three hollow-fiber spinnerets employed in this work (D/d1/d2 = 0.5/0.28/0.15 mm, 0.8/0.4/0.2 mm, and 1.4/0.9/0.6 mm) and their orifice gaps were 110, 200, and 250 μm, respectively. Unlike the wet-spinning of hollow fibers in which the inner channel of the spinneret accommodates bore fluids, in this work the inner channel was kept empty and no bore fluid was used. The processing temperature should be lower than the degradation temperature of PSF-*b*-PEG, and higher than its glass transition temperature (T_g). To identify a proper temperature, a series of temperatures ranged from 160°C to 210°C were explored. As the extruder is composed of two cavities as shown in Fig. 1, we set different temperatures to the two cavities and the upper cavity was always set 10 °C cooler than the lower cavity. The set temperature was described in the form of 160/170°C, for example.

The mixture of 80% *n*-propyl alcohol and 20% acetone (w/w) (80% Pa + 20% Ac) was used as the swelling agent according to our previous study on the selective swelling of PSF-*b*-PEG thin films. The extruded hollow fibers were immersed in the swelling agent for a certain duration at a fixed temperature followed by post treatment and drying at 40 °C for 1 h, thus finishing the preparation of HFMs of PSF-*b*-PEG.

2.3. Characterizations

The morphologies of HFMs were characterized by the scanning electron microscopy (SEM, Hitachi S4800). The inner surface of HFMs was exposed by lengthwise cutting the HFMs. To obtain the cross-sectional sample, HFMs were immersed in isopropanol for several seconds, then quick-frozen in liquid nitrogen and fractured. Nitrogen adsorption/desorption analysis was performed on a surface area and porosity analyzer (Micromeritics, ASAP-2020) at 77 K, and samples

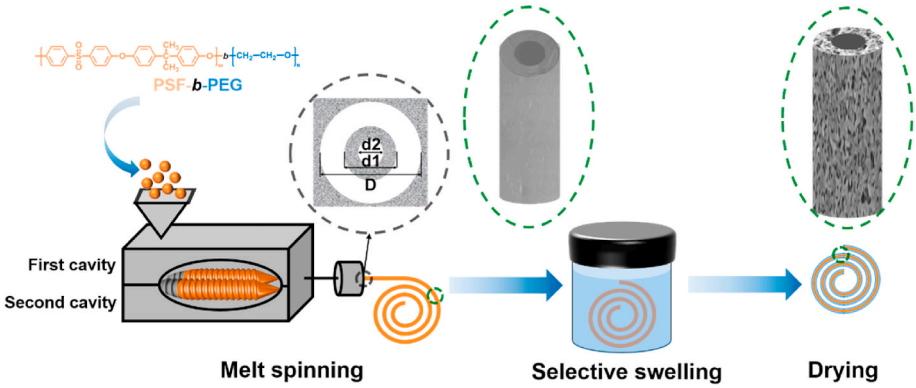

Fig. 1. The schematic diagram of the preparation of HFMs of PSF-*b*-PEG by melt spinning and selective swelling.

were degassed in vacuum at 100 °C for 12 h. The tensile properties of HFMs were evaluated with an electronic universal testing system (CMT6023, Shenzhen SANS). HFMs with a length of 10 cm were used for tensile testing. The tensile stress (MPa) and strain (%) at break were calculated by Eqs. (1) and (2), respectively.

$$Stress = \frac{P}{A} \tag{1}$$

where P (N) is the maximum load, A (mm^2) is the initial cross-sectional area of HFMs.

$$Strain = \frac{\Delta l}{l} \times 100\% \tag{2}$$

where Δl (mm) and l (mm) are the displacement value at break and the initial testing length of HFMs, respectively.

The porosity (%) of the HFMs was determined comparing the density of the fibers before and after swelling treantment using Eq. (3):

$$Porosity = \left(1 - \frac{\rho_1}{\rho_0}\right) \times 100\% \tag{3}$$

where ρ_0 (g/cm^3) and ρ_1 (g/cm^3) are the densities of HFMs before and after swelling. ρ_0 and ρ_1 were calculated by Eq. (4):

$$\rho = \frac{m}{\pi \times L \times (R^2 - r^2)} \tag{4}$$

where m (g) and L (cm) are the mass and length of HFMs, respectively, which are considered to be constant during swelling, R (cm) and r (cm) are the outer and inner radius, respectively.

2.4. Filtration tests

The pure water permeance (PWP) and rejection were tested using a homemade cross-flow filtration device. Before testing, HFMs were sealed in a polyurethane tube (PU tube, 8 × 12 mm) with the hot melt adhesive. The HFMs were pre-pressed at 2 bar for 10 min to obtain a stable permeance. Afterwards, the HFMs were tested at 2 bar for 5 min. The PWP was calculated by Eq. (5).

$$PWP = \frac{V}{\pi \times d \times l \times t \times \Delta P} \tag{5}$$

where PWP ($L{\cdot}m^{-2}{\cdot}h^{-1}{\cdot}bar^{-1}$) represents the membrane permeance for pure water, V (L) is the volume of pure water passing through the HFMs. d (m) is the outer diameter of HFMs, l (m) is the effective tested length of HFMs, t (h) is the testing time, and ΔP (bar) is the operation pressure.

BSA was selected as the retention substance to evaluate the separation performance of HFMs. BSA was dissolved in PBS at a concentration of 0.5 $g{\cdot}L^{-1}$. BSA rejection tests were performed at 25°C with a 2 $L{\cdot}min^{-1}$ cross-flow rate for the feed solutions. After 10 min testing, 3 mL solution was taken on the permeation side as the permeation solution. The BSA concentrations in the feed and permeation solutions were measured by a UV–Vis spectrometer (NanoDrop 2000C, Thermo Scientific) at the wavelength of 280 nm. The BSA rejection (R, %) was calculated by Eq. (6).

$$R(\%) = \left(\frac{C_f - C_p}{C_f}\right) \times 100\% \tag{6}$$

where C_p and C_f are the BSA concentrations ($g{\cdot}L^{-1}$) in the permeation and the feed solutions, respectively. The BSA rejection in this work were the observed sieving coefficient [33].

3. Results and discussions

3.1. Melt spinning PSF-b-PEG to prepare hollow fibers

Because it is the first time to use the BCP material, PSF-*b*-PEG, to prepare hollow fibers *via* melt spinning, we first examined the processing parameters of melt spinning in detail. Among the parameters, the spinning temperature is the most important one, which determines the fluidity of BCPs. The selected temperatures were between the T_g of PSF-*b*-PEG (~190°C for PSF [34] and ~ -60°C for PEG [35]) and its degradation temperature, and orifice gaps was 250 μm. High temperatures, such as 200/210°C, PSF-b-PEG exhibited excessive fluidity, lead to an uncontrolled spinning speed of about 75 mm/min and melt fracture during extrusion. As a consequence, the spun hollow fibers presented a corrugated outer surface, and defects like large voids appeared in the cross section (Figs. S1a and S1b). When the spinning temperature was decreased to 170/180°C, the fluidity of PSF-b-PEG melt was appropriate with a spinning speed of 15 mm/min, thus producing uniform hollow fibers with smooth surfaces (Fig. 2a–c). With the spinning temperature further decreased to 160/170°C, the spinning process could not proceed continuously and was interrupted, although the hollow fibers without defect were obtained (Figs. S1c and S1d). Therefore, the optimum spinning temperature was determined to be 170/180°C.

The wall thicknesses of hollow fibers not only greatly influence the performance of HFMs, but also determine their mechanical properties. Therefore, we spun hollow fibers with different wall thickness using three spinnerets with the orifice gaps of 110 μm, 200 μm and 250 μm. The appearance of hollow fibers with different thicknesses is shown in Fig. 2a, d, 2g. These hollow fibers had no obvious difference in appearance and all were brown, which was close to the color of the PSF-*b*-PEG raw material. As shown in Fig. 2 and Fig. S2, the outer surfaces, inner surfaces and the cross sections were all dense and free of defects for the three hollow fibers. From the cross-sectional SEM images, the wall thicknesses of these hollow fibers were determined to be 254, 207, and 115 μm, respectively. Clearly, the wall thicknesses are only slightly larger than the theoretical values, the orifice gaps ($D/2$-$d_1/2$) of the

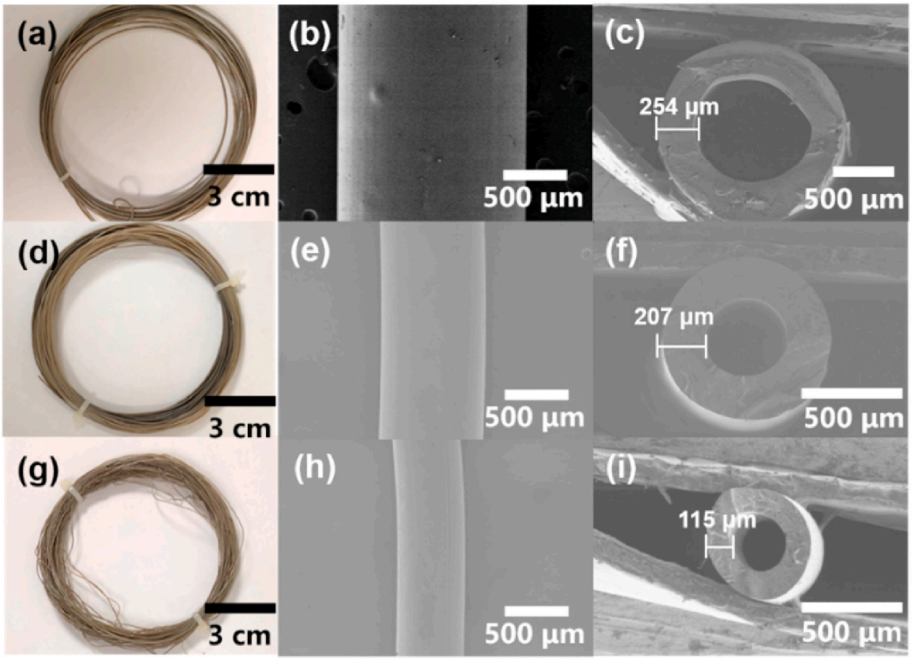

Fig. 2. The photograph (a, d, g) and SEM micrographs of the surfaces (b, e, h) and cross sections (c, f, i) of the hollow fibers spun using spinnerets with different orifice gaps: 250 μm (a–c), 200 μm (d–f) and 110 μm (g–i).

spinnerets, as a result of the effect of extrusion swell. These results indicate that PSF-*b*-PEG has good melt processibility and well-structured hollow fibers with different diameters can be continuously spun by extruding PSF-*b*-PEG melts through the corresponding spinnerets. This should be attributed to the presence of PEG which is soft and has a low T_g in the block copolymer. Although PSF is a rigid polymer with a T_g as high as ~190°C, the homogeneous mixture of PEG to the molecular level in the PSF matrix with a considerable weight ratio (~21%) reduces the rigidity of PSF-*b*-PEG, making it ductile and fluidizable at temperatures lower than the T_g of PSF.

3.2. Selective swelling of hollow fibers to prepare HFMs

The spun hollow fibers with different diameters were subsequently cavitated following the mechanism of selective swelling-induced pore generation [10] to prepare HFMs. According to our previous studies on the selective swelling behavior of PSF-*b*-PEG [34], all hollow fibers were subjected to swelling treatment in the mixture of 80% *n*-propyl alcohol and 20% acetone (w/w) (80% Pa + 20% Ac) at 65°C for 1 h. For convenience, we use HFM-*X* to represent the HFM spun by the spinneret with an orifice gap of *X* μm in the following discussion (Table 1).

After swelling, the brown HFMs turned into milky white (Fig. 3a), indicating the formation of pores in the HFMs. The inner and outer surfaces as well as the cross sections all exhibited a three-dimensionally interconnected nanoporous structure (Fig. 3d–f). The interconnected structure is essential for membrane separation as it allows the transport of substances in the HFMs. Prepared under the identical swelling condition, HFMs with different wall thicknesses all possess a highly porous structure with a similar interconnected porous morphology (Fig. 3, Fig. S3 and Fig. S4). After swelling, the outer diameter of the HFM-110 was increased from 520 to 622 μm, and the inner diameter was increased from 290 to 326 μm. Hence, the change of the wall thickness was the result of the increase both in the outer and the inner diameters of the fibers. After swelling, the wall thicknesses of the three fibers were increased to 148, 257, and 302 μm, respectively (Table 1). There is an increase in wall thickness of 18.9–28.7% as a result of the formation of numerous nanopores throughout the fiber walls.

Table 1
The parameters of PSF-*b*-PEG HFMs with different diameters.

Samples	Orifice gap /μm	Wall thickness/μm		Surface area /(m^2/g)	Pore volume /(cm^3/g)	Pore size /nm
		Before swelling	After swelling			
HFM-110	110	115	148	16.8	0.050	14.5
HFM-200	200	207	257	14.4	0.061	18.0
HFM-250	250	254	302	20.1	0.098	20.2

We then characterized the porous properties of HFMs by nitrogen adsorption/desorption analysis. The nitrogen adsorption/desorption isotherms of HFMs (Fig. S5) all presented the typical Langmuir type IV with a typical hysteresis loop at high pressure [36], indicating the mesoporous structure of the produced HFMs. As shown in Table 1, the mean pore sizes of the three HFMs were 14.5, 18.0, and 20.2 nm, respectively, indicating that thicker fibers exhibited bigger pores. For flat-sheet BCP films, changes in film thickness were not observed to notably influence pore sizes during the process of selective swelling-induced pore generation [34]. In contrast, for hollow fibers, the fiber walls are curved, thus constraining the volume expansion of the BCP during swelling. HFM-110 is the thinnest fiber and possesses the largest curvature, and consequently its volume expansion is suppressed to the largest degree, thus producing smallest pores after finishing the swelling process upon drying. Similarly, selective swelling of HFM-200 and HFM-250 with increasing fiber diameters produces larger pores as a result of weaker constraint on volume expansion.

Due to the difference in the pore size and wall thickness, the separation properties of these HFMs obviously varied. As shown in Fig. 4a, with the decrease of wall thickness, the permeance was increased from 39.6 to 65.5 $L{\cdot}m^{-2}{\cdot}h^{-1}{\cdot}bar^{-1}$ while the BSA rejection was also increased, from 20.9 to 55.5%. The permeance increase should be mainly attributed to the decrease of mass transfer resistance as a result of decreased wall thickness. Although decrease in pore sizes will reduce permeability, it seems playing a minor role in determining the water permeance compared to the influence of changes in wall thickness in this case.

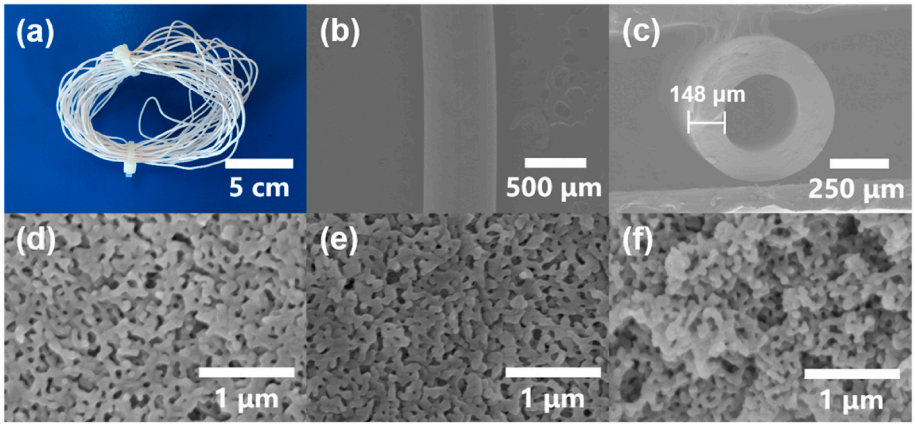

Fig. 3. The photograph (a) and SEM micrographs (b–f) of the HFM-110 membrane: the surface (b), the cross section (c), and the enlarged view of the outer surface (d), the inner surface (e) and the cross section (f).

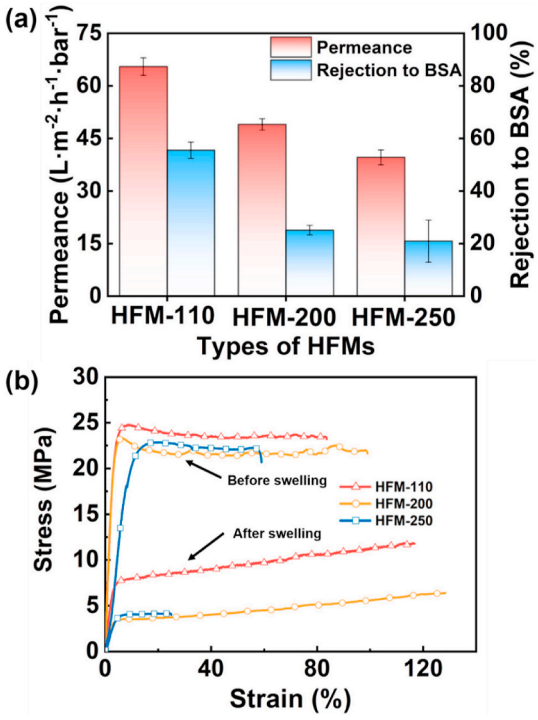

Fig. 4. The permeance and rejection to BSA of HFMs with different diameters (a) and the strain−stress curves of hollow fibers before and after swelling (b).

Oppositely, the change in pore size is more sensitive to rejections, and smaller pores give higher BSA rejections. Therefore, the permeance and BSA rejection are both increased with decreasing diameters of HFMs.

We then perform tensile tests of PSF-*b*-PEG hollow fibers before and after swelling to analyze their mechanical properties, and the results are shown in Fig. 4b Before swelling, the hollow fibers with different diameters displayed similar tensile strengths around 23 MPa and their elongations at rupture were in the range of 55–100%. After swelling, the tensile strengths of these hollow fibers were all reduced. The tensile strengths of HFM-110 and HFM-200 were reduced to 12.5 and 6.5 MPa, respectively, while their elongations at rupture were increased to 120 and 130%, respectively. However, the tensile strength and the elongation at rupture for the HFM-250 were reduced to 4.5 MPa and 25%, respectively. The decrease of tensile strength should be attributed to the presence of numerous pores in the fiber wall after swelling. Moreover, as shown in Table 1, thicker hollow fibers exhibited larger pore volumes, consequently leading to pronounced decrease in tensile strength. There is a balance between the strain and the rigidity. The rigidity of HFMs is gradually enhanced with the increase of wall thickness. When the wall thickness is larger than a certain degree, the excessive rigidity leads to the sharp fall of strain, which is the case of HFM-250. Notably, although the tensile strengths for HFMs after swelling were reduced, they are still much higher than that of HFMs prepared by the NIPS process (typically lower than 4 MPa [37]). Such an excellent mechanical robustness of PSF-*b*-PEG HFMs prepared by the melt spinning and selective swelling process can be ascribed to three factors. First, the intrinsic strong robustness of PSF consisting of the matrix of the hollow fibers guarantees the high strength of the fibers. Second, the highly flexible PEG blocks constituent the dispersed phases in the copolymer, providing ductileness to the hollow fibers. Third, the HFMs contain only uniform nanoscale pores homogeneously distributed throughout the fiber walls and are free of any defects such as big voids frequently observed in membranes prepared by the phase inversion process, thus eliminating any possible weak points which may lead to mechanical failure. The above discussions reveal that HFMs with thinner wall thickness give better performances both in separation and mechanical properties. Therefore, the thinnest fibers, HFM-110, were used in our following studies.

3.3. *Effect of swelling parameters on HFM separation performances*

The swelling temperature plays a crucial role in the process of selective swelling-induced pore generation as temperature strongly influences the interaction between BCPs and swelling agents. We investigated the separation performances of HFM-110 membranes swelling treated in 80% Pa + 20% Ac at different temperatures for 1 h. The chosen swelling temperatures were far below the T_g of PSF to avoid structure collapse of the hollow fibers.

As shown in Fig. S6, swelling at any temperature between 55 and 70°C results in interconnected nanopores both in the outer and inner surface. Importantly, cross-sectional SEM images reveal that the interior of the fiber walls is also in a highly porous structure. When the swelling temperature was 55°C, a few irregular pore appeared on the outer surface. Further increasing the swelling temperature to 60°C, the size and number of pores were increased. The porous structure was well distributed on the entire outer surface, and more pores were connected with adjacent pores to form a network structure when HFMs were subjected to swelling at 65 and 70°C. The porous structure is formed through the mechanism of selective swelling-induced pore generation. For the PSF-*b*-PEG hollow fibers, the PEG microdomains are randomly distributed in the PSF matrix. During the swelling process, the rapid infiltration of *n*-propanol into the PEG microdomains causes the

expansion of the PEG microdomains. At the same time, PSF chains absorb acetone and gain moderately increased segmental mobility. The expanded PEG microdomains squeeze the PSF matrix to deform plastically, and merge with neighboring ones, leading to a continuous PEG phase distributed in the PSF matrix. In the subsequent drying process, the deformed PSF matrix cannot return to the original position due to the loss of mobility with the evaporation of acetone. Meanwhile, the swollen PEG chains collapse and pores are formed at the same position. Moreover, the collapsed PEG chains are enriched on the pore walls and membrane surface. The hydrophilic PEG chains can tightly bind water molecules *via* hydrogen bonding and form a protective hydration layer on the membrane surface and pore walls, which serves to minimize access to the interface for potential fouling [38]. Meanwhile, the covalent bonds between the PEG chains and PSF chains guarantee the long-term stability of this interface property [39].

As pore generation by selective swelling is a nondestructive process, in which pore formation is not at the sacrifice of a particular component from the pristine material to be swelling treated [8], the increase in volume of the fibers after swelling can be solely ascribed to the introduction of pores in the original nonporous walls of the hollow fibers. Furthermore, the porosities of the HFMs prepared under different swelling temperatures can be easily estimated by comparing the density of the fibers before and after swelling. As shown in Table S1 and Fig. 5a, the thickness and the corresponding porosity of the fiber walls continues increasing with rising swelling temperature. Swelling for 1 h at 55 and 70 °C is able to produce a porosity of 34.2% and 44.6%, respectively, indicating the efficiency of this selective swelling process if the swelling agents are appropriately selected.

The separation performances of HFMs prepared at different swelling temperatures are shown in Fig. 5b. With the temperature increased from 55 to 70°C, the permeance was nearly linearly increased from 13.7 to 119.3 $L{\cdot}m^{-2}{\cdot}h^{-1}{\cdot}bar^{-1}$, and the rejection to BSA was gradually reduced from 88.2 to 29.9%. The change of the HFMs performance can be easily explained by the increased porosity as a result of enlarged pores in the fiber walls of HFMs prepared at higher swelling temperatures.

The swelling duration also has an important influence on the performance of HFMs. During the swelling process, the swelling duration influences the volume of the swelling agents adsorbed in the PEG microdomains before the swelling reaches equilibrium. Typically, the more absorption, the higher swelling degree, and it would lead to the larger pore sizes and higher porosities. To investigate the influence of swelling duration, we investigated the separation performances of HFM-110 membranes swelling treated in 80% Pa+20% Ac at 65°C for different durations. As shown in Fig. S7, a swelling duration of 1 h is sufficient to produce a highly porous morphology throughout the entire structure of the hollow fibers, and the cross-sectional SEM images also reveal an interconnected porosity. We also measured the wall thickness of the hollow fibers prepared by swelling for different durations (Table S2), and found that a swelling duration of 1 h is able to produce a porosity of 39.2% (Fig. 5c), and further extending swelling does not significantly increase the porosity, implying that selective swelling is a relatively fast process to cativate the BCP hollow fibers.

Fig. 5d shows the permeance and rejection to BSA of HFMs swollen at different swelling durations. As the swelling duration rising from 1 h to 3 h, the permeance presented a linearly increasing trend from 65.5 to 122.2 $L{\cdot}m^{-2}{\cdot}h^{-1}{\cdot}bar^{-1}$, whereas the rejection to BSA was decreased from 55.5 to 22.6%. The permeance and rejection remained nearly unchanged with the swelling duration further extended to 5 h. The variation trend of the performance is consistent with the above morphological results. We note that, compared to HFMs membranes prepared by the SNIPS process [19], the BCP HFMs prepared in this work at the current stage exhibit moderate permselectivity. However, their performances are expected to be enhanced by annealing the BCP hollow fibers to perpendicularly align the PEG cylinders before selective swelling. This is because this treatment of swelling after annealing would produce uniform and straight pores penetrating through the entire wall of the fibers, favoring fast and selective separation [40]. However, they show much better permeance than polyolefin HFMs by cold stretching [41]. The polyolefin HFMs prepared by cold stretching are limited by their strong hydrophobicity and cannot be directly used for water treatment.

We investigated the pressure-resisting property of the PSF-*b*-PEG HFMs by testing the pure water fluxes under different pressures. As shown in Fig. 6, the flux was almost linearly increased with the pressure increased from 0.5 to 6.0 bar. The water flux began to decline when the pressure exceeded 6.0 bar, implying the compaction of the membrane

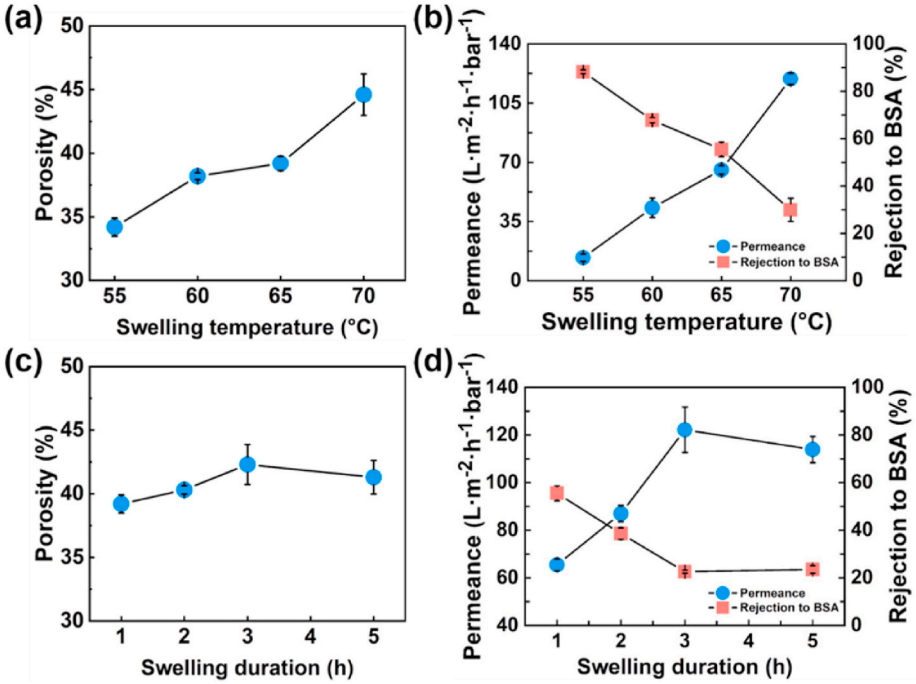

Fig. 5. The porosity, permeance and rejection to BSA of HFM-110 membrane swollen at different temperatures (a, b) and swollen for different durations (c, d).

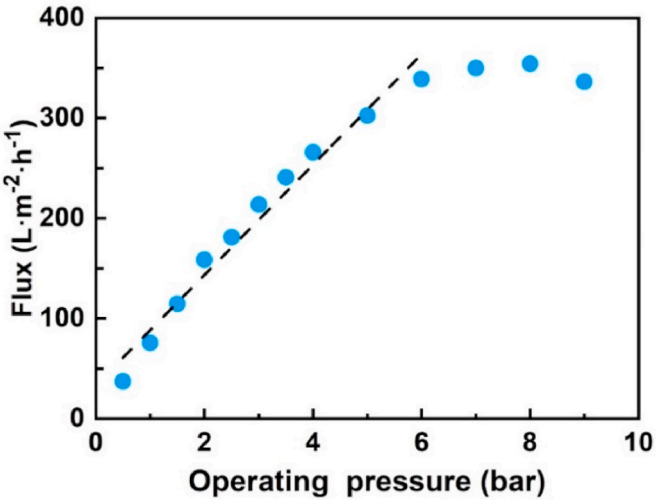

Fig. 6. Water fluxes of HFM-110 membrane under different pressures.

porosity. However, we did not observe any sudden increase in water flux within the testing range of pressures, suggesting that the HFM is robust enough to withstand a pressure as high as at least 9.0 bar without any fracture.

It should be noted that melt spinning coupled with selective swelling is a "cleaner" strategy for the preparation of HFMs. Melt spinning does not require the use any solvents, avoiding potential environmental and health risks. In the selective swelling step, organic solvents are used as the swelling agents. However, the swelling agents are used in fully closed environments and can be directly reused for repeated times as nothing is left in the swelling bath. Therefore, the risks in usages of organic solvents in the selective swelling process is minimized. Moreover, neither melt spinning nor selective swelling produce any waste water, which is in strong contrast to the phase inversion processes, i.e. NIPS. Additionally, benefit from the non-destructive and additive-free nature of the selective swelling, BCPs used in the preparation of HFMs by this process can be recycled as raw material and reused. Also importantly, compared with polyolefin HFMs prepared by cold stretching, the HFMs prepared in this work by melt spinning and selective swelling are inherently hydrophilic and fouling resistant, which can be directly used in water treatment and in other separation processes in the aqueous milieu. As discussed earlier, further efforts should be made to improve the permeability of these HFMs.

4. Conclusions

In summary, we develop a new method to fabricate BCP HFMs by combining melt spinning and selective swelling. Melt spinning first prepares defect-free, dense hollow fibers of an affordable and robust block copolymer, PSF-*b*-PEG, then selective swelling produces interconnected nanoporosity in fiber walls. Melt spinning can be smoothly proceeded at the temperature lower than the T_g of PSF because of the presence of highly flexible PEG in the copolymer. We spun hollow fibers with various diameters and wall thicknesses by using spinnerets with corresponding orifice gaps. Selective swelling in the mixture of 80% *n*-propyl alcohol and 20% acetone (w/w) transforms the dense hollow fibers to HFMs with interconnected porosities. Swelling temperatures and durations influence the morphology and consequently the separation properties of the HFMs. There is a curvature effect in the selective swelling of hollow fibers and thinner fibers exhibit smaller pores after swelling under the same condition. It is found that the HFM with the thinnest fiber wall exhibits best performances in both permeability and selectivity because of the less mass transfer resistance and smaller pore sizes. Furthermore, the HFMs show excellent mechanical robustness and pressure resistance as a result of the coexistence of strong PSF and flexible PEG in the membranes. This process does not use organic solvents to dissolve the polymer and the swelling agent can be directly reused, therefore, it is a "cleaner" process compared to solvent-extensive phase inversion processes in the manufacturing HFMs. This work not only provides a new method to prepare the BCP HFMs, but also demonstrates a "cleaner" process to prepare HFMs for ultrafiltration applications.

Author statement

Dinglei Zhong: Investigation, Data analysis, Writing-orginal draft. Jiemei Zhou: Data analysis, Writing-review & editing. Yong Wang: Conceptualization, Supervision, Writing-review & editing. All authors have approved to the final version of the manuscript.

Declaration of competing interest

The authors declare the following financial interests/personal relationships which may be considered as potential competing interests: Nanjing Tech University has filed the patent application related to the findings described in this manuscript.

Acknowledgments

Financial support from the National Natural Science Foundations of China (21776126, 21825803) are gratefully acknowledged.

Appendix A. Supplementary data

Supplementary data to this article can be found online at https://doi.org/10.1016/j.memsci.2021.119374.

References

[1] D.A. Olson, L. Chen, M.A. Hillmyer, Templating nanoporous polymers with ordered block copolymers, Chem. Mater. 20 (2008) 869–890.
[2] V. Abetz, P.F.W. Simon, Phase behaviour and morphologies of block copolymers, Block Copolymers I 189 (2005) 125–212.
[3] S.B. Darling, Directing the self-assembly of block copolymers, Prog. Polym. Sci. 32 (2007) 1152–1204.
[4] T.P. Lodge, Block copolymers: long-term growth with added value, Macromolecules 53 (2020) 2–4.
[5] M. Radjabian, V. Abetz, Advanced porous polymer membranes from self-assembling block copolymers, Prog. Polym. Sci. 102 (2020), 101219.
[6] E.A. Jackson, Y. Lee, M.R. Radlauer, M.A. Hillmyer, Well-ordered nanoporous ABA copolymer thin films *via* solvent vapor annealing, homopolymer blending, and selective etching of ABAC tetrablock terpolymers, ACS Appl. Mater. Interfaces 7 (2015) 27331–27339.
[7] V. Abetz, Isoporous block copolymer membranes, Macromol. Rapid Commun. 36 (2015) 10–22.
[8] Y. Wang, C.C. He, W.H. Xing, F.B. Li, L. Tong, Z.Q. Chen, X.Z. Liao, M. Steinhart, Nanoporous metal membranes with bicontinuous morphology from recyclable block-copolymer templates, Adv. Mater. 22 (2010) 2068–2072.
[9] S. Rangou, K. Buhr, V. Filiz, J.I. Clodt, B. Lademann, J. Hahn, A. Jung, V. Abetz, Self-organized isoporous membranes with tailored pore sizes, J. Membr. Sci. 451 (2014) 266–275.
[10] Y. Wang, Nondestructive creation of ordered nanopores by selective swelling of block copolymers: toward homoporous membranes, Acc. Chem. Res. 49 (2016) 1401–1408.
[11] W. Sun, Z. Wang, X. Yao, L. Guo, X. Chen, Y. Wang, Surface-active isoporous membranes nondestructively derived from perpendicularly aligned block copolymers for size-selective separation, J. Membr. Sci. 466 (2014) 229–237.
[12] Z. Wang, R. Liu, Q. Lan, Y. Wang, Selective swelling blends of block copolymers for nanoporous membranes with enhanced permeability and robustness, J. Polym. Sci. B Polym. Phys. 55 (2017) 1617–1625.
[13] H. Yang, J. Zhou, Z. Wang, X. Shi, Y. Wang, Selective swelling of polysulfone/poly (ethylene glycol) block copolymer towards fouling-resistant ultrafiltration membranes, Chin. J. Chem. Eng. 28 (2020) 98–103.
[14] Y. Zhang, N.E. Almodovar-Arbelo, J.L. Weidman, D.S. Corti, B.W. Boudouris, W. A. Phillip, Fit-for-purpose block polymer membranes molecularly engineered for water treatment, npj Clean Water (2018) 1.
[15] R. Hilke, N. Pradeep, A.R. Behzad, S.P. Nunes, K.-V. Peinemann, Block copolymer/homopolymer dual-layer hollow fiber membranes, J. Membr. Sci. 472 (2014) 39–44.

[16] R. Hilke, N. Pradeep, P. Madhavan, U. Vainio, A.R. Behzad, R. Sougrat, S.P. Nunes, K.V. Peinemann, Block copolymer hollow fiber membranes with catalytic activity and pH-response, ACS Appl. Mater. Interfaces 5 (2013) 7001–7006.
[17] K. Sankhala, D.C.F. Wieland, J. Koll, M. Radiabian, C. Abetz, V. Abetz, Self-assembly of block copolymers during hollow fiber spinning: an in situ small-angle X-ray scattering study, Nanoscale 11 (2019) 7634–7647.
[18] L. Xia, J. Ren, J.R. McCutcheon, Braid-reinforced thin film composite hollow fiber nanofiltration membranes, J. Membr. Sci. 585 (2019) 109–114.
[19] K. Sankhala, J. Koll, M. Radjabian, U.A. Handge, V. Abetz, A pathway to fabricate hollow fiber membranes with isoporous inner surface, Adv. Mater. Interfaces (2017) 4.
[20] N. Noor, J. Koll, C. Abetz, H. Notzke, V. Abetz, Continuous production of macroporous films: an alternative to breath figure assembly, Sci. Rep. 7 (2017).
[21] Y. Liu, T. Liu, Y. Su, H. Yuan, T. Hayakawa, X. Wang, Fabrication of a novel PS4VP/PVDF dual-layer hollow fiber ultrafiltration membrane, J. Membr. Sci. 506 (2016) 1–10.
[22] Y. Pang, J. Yang, T.E. Curtis, S. Luo, D. Huang, Z. Feng, J.O. Morales-Ferreiro, P. Sapkota, F. Lei, J. Zhang, Q. Zhang, E. Lee, Y. Huang, R. Guo, S. Ptasinska, R. K. Roeder, T. Luo, Exfoliated graphene leads to exceptional mechanical properties of polymer composite films, ACS Nano 13 (2019) 1097–1106.
[23] J. Zhao, L. Shi, C.H. Loh, R. Wang, Preparation of PVDF/PTFE hollow fiber membranes for direct contact membrane distillation *via* thermally induced phase separation method, Desalination 430 (2018) 86–97.
[24] K. Sankhala, J. Koll, V. Abetz, Setting the stage for fabrication of self-assembled structures in compact geometries: inside-out isoporous hollow fiber membranes, ACS Macro Lett. 7 (2018) 840–845.
[25] S. Mosadegh-Sedghi, D. Rodrigue, J. Brisson, M.C. Iliuta, Highly hydrophobic microporous low-density polyethylene hollow fiber membranes by melt-extrusion coupled with salt-leaching technique, Polym. Adv. Technol. 24 (2013) 584–592.
[26] A.A.I.A.S. Komaladewi, S. Anisah, A.K. Wardani, I.W. Surata, I.D.G.A. Subagia, I. G. Wenten, The effect of annealing and stretching parameters on the structure and performance of polypropylene hollow fiber membrane, Mater. Res. Express 6 (2019) 54001–54009.
[27] J. Jia, G. Kang, T. Zou, M. Li, M. Zhou, Y. Cao, Sintering process investigation during polytetrafluoroethylene hollow fibre membrane fabrication by extrusion method, High Perform. Polym. 29 (2017) 1069–1082.
[28] Z. Wang, X. Yao, Y. Wang, Swelling-induced mesoporous block copolymer membranes with intrinsically active surfaces for size-selective separation, J. Mater. Chem. 22 (2012) 20542–20548.
[29] Z. Wang, L. Guo, Y. Wang, Isoporous membranes with gradient porosity by selective swelling of UV-crosslinked block copolymers, J. Membr. Sci. 476 (2015) 449–456.
[30] Y. Wang, Y. Qin, A. Berger, E. Yau, C. He, L. Zhang, U. Gösele, M. Knez, M. Steinhart, Nanoscopic morphologies in block copolymer nanorods as templates for atomic-layer deposition of semiconductors, Adv. Mater. 21 (2009) 2763–2766.
[31] X. Shi, X. Wang, Y. Wang, Y. Wang, Producing nanoporosities in block copolymers within 30 s by microwave-boosted selective swelling, Macromolecules 53 (2020) 3619–3626.
[32] J. Zhou, Y. Wang, Selective swelling of block copolymers: an upscalable greener process to ultrafiltration membranes? Macromolecules 53 (2019) 5–17.
[33] M.P. Dugas, G. Van Every, B. Park, J.R. Hoffman, R.J. LaRue, A.M. Bush, Y. Zhang, J.L. Schaefer, D.R. Latulippe, W.A. Phillip, Resilient hollow fiber nanofiltration membranes fabricated from crosslinkable phase-separated copolymers, Mol. Syst. Des. Eng. 5 (2020) 943–953.
[34] Z.G. Wang, R. Liu, H. Yang, Y. Wang, Nanoporous polysulfones with in situ PEGylated surfaces by a simple swelling strategy using paired solvents, Chem. Commun. 53 (2017) 9105–9108.
[35] M.A. Webb, Y. Jung, D.M. Pesko, B.M. Savoie, U. Yamamoto, G.W. Coates, N. P. Balsara, Z.-G. Wang, T.F. Miller, Systematic computational and experimental investigation of lithium-ion transport mechanisms in polyester-based polymer electrolytes, ACS Cent. Sci. 1 (2015) 198–205.
[36] Z. Liang, B. Sun, X. Xu, H. Cui, J. Tian, Metallic 1T-phase MoS_2 quantum dots/g-C_3N_4 heterojunctions for enhanced photocatalytic hydrogen evolution, Nanoscale 11 (2019) 12266–12274.
[37] X.S. Li, C.H. Loh, R. Wang, W. Widjajanti, J. Torres, Fabrication of a robust high-performance FO membrane by optimizing substrate structure and incorporating aquaporin into selective layer, J. Membr. Sci. 525 (2017) 257–268.
[38] S.B. Darling, Perspective: interfacial materials at the interface of energy and water, J. Appl. Phys. 124 (2018), 030901.
[39] D. Zhong, Z. Wang, J. Zhou, Y. Wang, Additive-free preparation of hemodialysis membranes from block copolymers of polysulfone and polyethylene glycol, J. Membr. Sci. 618 (2021), 118690.
[40] W. Sun, Z.G. Wang, X.P. Yao, L.M. Guo, X.Q. Chen, Y. Wang, Surface-active isoporous membranes nondestructively derived from perpendicularly aligned block copolymers for size-selective separation, J. Membr. Sci. 466 (2014) 229–237.
[41] K.L. Li, Y. Zhang, L.L. Xu, F.F. Zeng, D.Y. Hou, J. Wang, Optimizing stretching conditions in fabrication of PTFE hollow fiber membrane for performance improvement in membrane distillation, J. Membr. Sci. 550 (2018) 126–135.